Sudden pressure enhancement and tailward retreat in the near-Earth plasma sheet: THEMIS observation and MHD simulation

AUTHOR(S):

Yao, Y.; Ebihara, Y.; Tanaka, T.

CITATION:

Yao, Y. ...[et al]. Sudden pressure enhancement and tailward retreat in the near-Earth plasma sheet: THEMIS observation and MHD simulation. Journal of Geophysical Research A: Space Physics 2015, 120(1): 201-211

ISSUE DATE:

2015-01

URL:

http://hdl.handle.net/2433/237233

AGU PUBLICATIONS
JGR
Journal of Geophysical Research: Space Physics

RESEARCH ARTICLE
10.1002/2014JA020482

Key Points:
- THEMIS observed tailward retreat of high-pressure region after substorm onset
- MHD result shows that high-pressure region retreats tailward at off equator
- Convergence of plasma flow responsible to high-pressure region tailward retreat

Supporting Information:
- Readme
- Figure S1
- Figure S2
- Figure S3
- Figure S4
- Figure S5
- Figure S6
- Figure S7
- Figure S8
- Figure S9
- Figure S10
- Figure S11
- Figure S12
- Figure S13
- Text S1
- Text S2
- Text S3
- Text S4

Correspondence to:
Y. Yao,
yyao0103@gmail.com

Citation:
Yao, Y., Y. Ebihara, and T. Tanaka (2015), Sudden pressure enhancement and tailward retreat in the near-Earth plasma sheet: THEMIS observation and MHD simulation, *J. Geophys. Res. Space Physics*, *120*, 201–211, doi:10.1002/2014JA020482.

Received 6 AUG 2014
Accepted 10 DEC 2014
Accepted article online 17 DEC 2014
Published online 15 JAN 2015

Sudden pressure enhancement and tailward retreat in the near-Earth plasma sheet: THEMIS observation and MHD simulation

Y. Yao[1], Y. Ebihara[1], and T. Tanaka[2]

[1]Research Institute for Sustainable Humanosphere, Kyoto University, Uji, Japan, [2]Kyushu University, Fukuoka, Japan

Abstract Sudden enhancement of the plasma pressure in the near-Earth plasma sheet is one of the common manifestations of substorms and is thought to play an important role in relevant disturbances in the magnetosphere and ionosphere. On 1 March 2008, four of the Time History of Events and Macroscale Interactions during Substorms probes observed the sudden enhancement of the plasma pressure around 15:40 UT. The four probes were almost aligned along the Sun-Earth line, which was suitable for investigating spatial-temporal evolution of the near-Earth plasma sheet around the substorm onset. The four probes were located off the equatorial plane, according to a magnetic field model. The plasma pressure suddenly increased at the innermost probe first (at ~7.2 *Re*), followed by the outer probes (at ~7.5, ~8.3, and ~10.4 *Re*), that could be seen as a tailward propagation (or retreat) of high-pressure region (HPR). After comparing with results of a global magnetohydrodynamic simulation, we found that only the tailward propagation of the HPR could be seen at off equator. Near the equatorial plane, the HPR propagates earthward from the magnetotail region, then it retreats tailward. In the course of the tailward retreat, the HPR also propagates away from the equatorial plane. As a consequence, the innermost probe observed the pressure enhancement first, followed by the outer probes. The propagation of the HPR in the Z_{GSM} direction is understood to be a combination of the convergence of the plasma flow (the divergence of bulk velocity along the Z_{GSM} axis) and the pressure gradient force.

1. Introduction

Variation of the plasma pressure is a characteristic feature around substorm onset. Statistical studies on the pressure variation were carried out previously in the plasma sheet [*Baumjohann et al*., 1989, 1991; *Wang et al*., 2001] and in the magnetotail [*Baumjohann*, 2002; *Yamaguchi et al*., 2004; *Wing et al*., 2007]. As indicated by *Baumjohann* [2002], adiabatic convective motion would lead to greatly high pressure of associated flux tubes closer to the Earth. Observation in the inner magnetosphere was reported to show simultaneous pressure enhancement and magnetic depression at the onset by CRRES satellite [*Sergeev et al*., 1998]. *Xing et al*. [2011] showed that a substantial duskward enhancement in the plasma sheet pressure gradient at 11 *Re* near the substorm onset on the basis of Time History of Events and Macroscale Interactions during Substorms (THEMIS) observations could be associated with enhanced upward field-aligned current during the late growth phase. *Xing et al*. [2012] further found that within 2 min prior to the onset, the ion distribution function showed a substantial earthward shift, which agrees with the ion acceleration ahead of the earthward convection dipolarization front.

Tanaka et al. [2010] performed a global magnetohydrodynamic (MHD) simulation and emphasized the importance of plasma pressure in the near-Earth plasma sheet in causing magnetospheric and ionospheric substorms. During the growth phase of a substorm, the balance between tailward pressure gradient force ($-\nabla P$) and earthward tension force ($(\mathbf{B}\cdot\nabla)\mathbf{B}/\mu_0$) in the plasma sheet is strictly satisfied, where P is the plasma pressure, $\mathbf{B}$ is the magnetic field, and μ_0 is the magnetic constant. As the growth phase proceeds, a near-Earth neutral line (NENL) forms, which results in the force imbalance. Just before the substorm onset, midtail region is always in the over tension state because of reduction of the pressure gradient force. The over tension state generates earthward fast flow. The convergence of the thermal energy flux contributes to the generation of high-pressure region (HPR) in the inner region from $X_{GSM} = -6$ to -8 *Re* within 3 or 4 min before the onset. As a consequence, the HPR propagates earthward before the onset. It was considered that the advection plays an important role in causing the pressure enhancement. The generation of the HPR results in a negative excursion

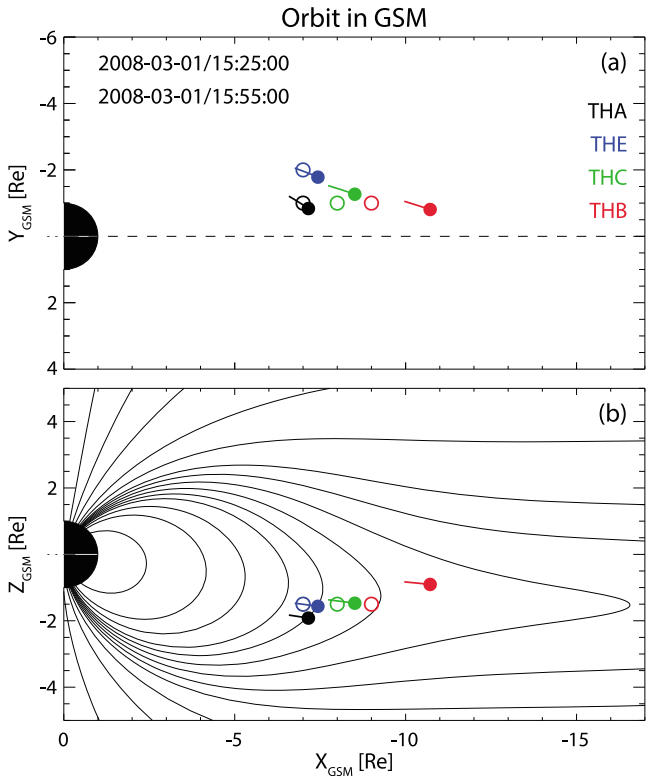

Figure 1. Orbit of THEMIS probes shown by solid circle (start point) with line in (a) X_{GSM}-Y_{GSM} and (b) X_{GSM}-Z_{GSM} planes during the period between 15:25 and 15:55 UT on 1 March 2008. The open circles refer to approximate positions of the THEMIS probes in MHD simulation domain (see text for details).

of B_Z and dipolarization due to diamagnetic current ($\mathbf{J} = \mathbf{B} \times \nabla P/B^2$). The generation of the diamagnetic current results in an intensification of the Region 2 field-aligned currents, together with the Region 1 currents on the nightside, and then auroral electrojets, namely, a substorm onset. Just after the onset, the HPR retreats tailward. The convergence of the bulk flow energy flux produces the secondary peak of the pressure outside the prime peak of the HPR. The pressure at the secondary peak is smaller than that at the prime one, so that the bulk flow energy, namely, the flow braking, may not contribute to the formation of the prime peak. The secondary peak also retreats tailward because of the tailward motion of the flow braking point. To our best knowledge, the evolution of the HPR in the near-Earth plasma sheet has not been clearly identified, in spite of the importance of the HPR in evolution of substorms as suggested by *Tanaka et al*. [2010].

The Time History of Events and Macroscale Interactions during Substorms (THEMIS) [*Angelopoulos*, 2008] probe constellation provides a unique opportunity to investigate substorm time changes of near-Earth plasma sheet. During the substorm taking place on 1 March 2008, four THEMIS probes aligned along the Sun-Earth line and observed a sudden pressure enhancement (SPE) from innermost probe to outer ones, which implies tailward retreat of high-pressure region (HPR). The purpose of this paper is to investigate the SPE and the substorm time changes of the near-Earth plasma sheet by using the global MHD simulation together with the data from the THEMIS mission.

2. Observations

We focus on a sudden pressure enhancement (SPE) taking place in the near-Earth plasma sheet around 15:40 UT on 1 March 2008. Four THEMIS probes were distributed along X_{GSM} axis from ~−7 to ~−10 *Re* in the postmidnight sector shown in Figure 1a by solid circle as its start position with solid line indicating its orbit. Figure 1b shows locations of the probes in the X_{GSM}-Z_{GSM} plane, together with magnetic field lines provided by the T89 magnetic field model [*Tsyganenko*, 1989]. The four probes were located at off equator. Probe THA was located at −6.9, −1.0, and −1.9 *Re* and probe THE was at −7.1, −1.9, and −1.5 *Re* in the GSM coordinates, so that these two probes were located similarly in the X_{GSM} axis. Probe THE was about 1 *Re* far from probe THA in−Y_{GSM} direction. Probe THC was located at −8.1, −1.4, and −1.4 *Re*, which was about 1 *Re* tailward of the probe THA, and probe THB was located at −10.3, −0.9, and −0.9 *Re*. During the period of interest, particle data are unavailable on probe THD because of contamination from energetic particles. Therefore, we only use the observations from the other four probes.

By using an algorithm of automated detection of Pi2 pulsations, it is confirmed by *Nosé et al*. [1998] that there was a Pi2 pulsation at Kakioka station from 15:41 UT on 1 March 2008 with a duration of 2 min. A positive bay was recorded at Memanbetsu at 15:41 UT. We presume that sudden pressure enhancement (SPE) observed by THEMIS probes is associated with an onset of the (weak) substorm recorded on the

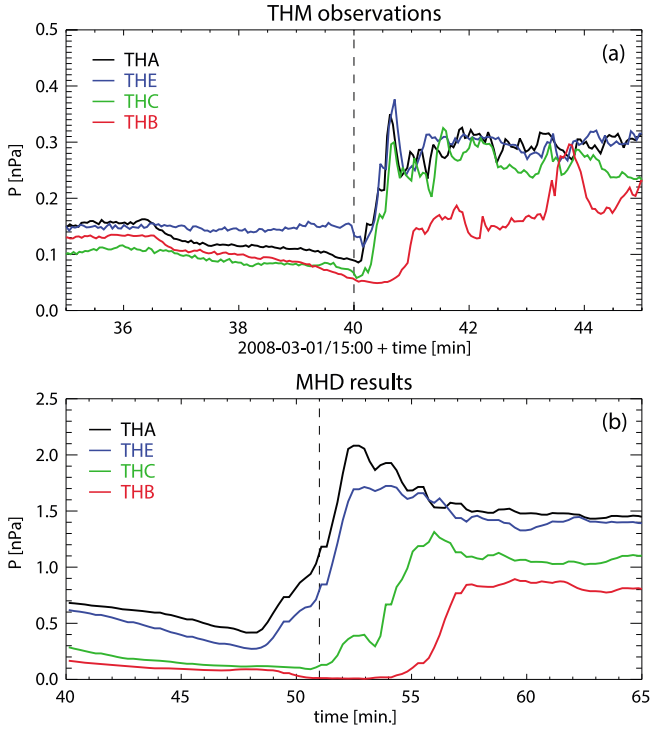

Figure 2. (a) Time series of ion pressure defined as $P_{ESA} + P_{SST}$ at probes THA, THE, THC, and THB corresponding to black, blue, green, and red lines, respectively. (b) Simulated plasma pressure at approximate positions of the THEMIS probes in MHD simulation domain (shown as open circles in Figure 1). The black, blue, green, and red lines indicate probes THA, THE, THC, and THB, respectively. The vertical dashed line in Figure 2a refers to the time point at 15:40 UT and in Figure 2b indicates the substorm onset at ~51 min.

ground at 15:41 UT. The Alfvén transit time from the magnetosphere to the ionosphere may result in a short delay between the SPE and the Pi2 pulsations observed on the ground. The *AL* index does not show a clear decrease around 15:41 UT probably due to a too narrow longitudinal extension of the auroral electrojet associated with this substorm.

Figure 2a shows time series of ion pressure observed by the THEMIS probes. The ion pressure is a combination of that obtained from particle spectrometers ESA (electrostatic analyzer) [*McFadden et al.*, 2008] (<25 keV) and SST (solid state telescope) [*Angelopoulos*, 2008] (>25 keV). Hereinafter, we call it the total ion pressure ($P_{ESA} + P_{SST}$). These four probes were located within a range from X_{GSM} ~−7 to −10 *Re* (Figure 1a). A noticeable feature is that the pressure increases with a significant time lag between the probes. Probes THA (black) and THE (blue) observed sudden pressure enhancement (SPE) almost simultaneously with largest magnitude, then followed by probes THC (green) and THB (red). Start time of the SPE at probes THA, THC, and THB were around 15:40:04, 15:40:15, and 15:40:54 UT, respectively. The probes were located close to their apogees, and the speed of the probes was slow, so that the time delay is most likely caused by a temporal change of the pressure, but not a spatial one. If the time delay of the SPEs results from the temporal change, Figure 2a will manifest a tailward propagation of the high-pressure region (HPR).

3. MHD Simulation

We used a global magnetohydrodynamic (MHD) simulation [*Tanaka et al.*, 2010] that has a capability of reproducing many observable manifestations of substorms, including the formation of a near-Earth neutral line (NENL) [*Baker et al.*, 1996], earthward flow in the plasma sheet, stretching and dipolarization of magnetic field, and sudden intensification of a westward electrojet at the auroral latitudes. Although non-MHD processes have been suggested to trigger a substorm [e.g., *Lui et al.*, 1999], the global MHD simulation reasonably describes the global structure and dynamics of the magnetosphere that evolves self-consistently to satisfy mass, momentum, and energy equations.

The parameters used to run the global MHD simulation are exactly the same as those used by *Ebihara and Tanaka* [2013]. That is, solar wind speed of 372.4 km/s, solar wind density of 10 cm^{-3}, and interplanetary magnetic field (IMF) B_Y of 4.33 nT and B_Z of −4.33 nT. A substorm onset occurred at an elapsed time of ~51 min as identified from the *AL* index [*Ebihara and Tanaka*, 2013]. The solar wind parameters used by the simulation are different from those during the interval of interest, that is, around 15:41 UT on 1 March 2008, but major characteristics of changes can be well reproduced as mentioned below. The simulation results are detailed by *Tanaka et al.* [2010] and *Ebihara and Tanaka* [2013]. To carry out a comparison between THEMIS observations and the global MHD simulation, we determined, by visual inspection, the closest points in the simulation

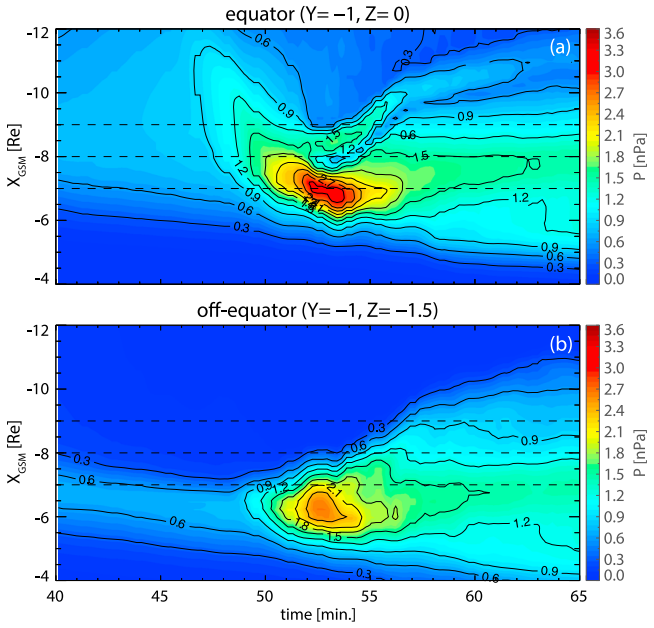

Figure 3. Temporal variation of simulated plasma pressure as a function of X_{GSM} (a) at equator ($Y_{GSM} = -1$ and $Z_{GSM} = 0$ *Re*) and (b) at off equator ($Y_{GSM} = -1$ and $Z_{GSM} = -1.5$ *Re*), respectively.

domain, at which both the THEMIS observations and the simulation results show most similar temporal variations in plasma pressure (P_P), magnetic pressure (P_B), and X component of velocity (V_X) (for more detailed comparisons, please refer to the supporting information), in particular, during the interval of sudden pressure enhancement (SPE). Open circles in Figure 1 show the positions that are approximately coincident with the THEMIS observations. In spite of different solar wind parameters, the approximately coincident positions are close to the THEMIS probes. The difference between the real position (solid circle) and coincident position (open circle) ranges from 0.3 *Re* for the probe THC and from 1.6 *Re* for the probe THB. The MHD simulation results are expected to be different from the observations because of the following reasons. First, solar wind parameters and IMF conditions are different from the observations. Second, tilt angle of the Earth's dipole is not taken into account in the simulation. Third, the simulation results depend on critical parameters, such as anomalous resistivity in the diffusion region, and ionospheric conductance. Our focus is largely on the large-scale changes of the plasma pressure in the near-Earth plasma sheet during the substorm. Reproducing exactly the observations is beyond the scope of this study.

Figure 2b demonstrates temporal variations of plasma pressure obtained at the most coincident positions of the THEMIS probes in the simulation domain. The plasma pressure suddenly increases first at the coincident position of probe THA (black), the innermost probe, followed by probes THE (blue), THC (green), and THB (red). The tailward propagation of the sudden pressure enhancement (SPE) is consistent with that observed from the THEMIS probes. The SPE occurs simultaneously at the probes THA and THE in the MHD simulation, which is roughly equal to the THEMIS observation shown in Figure 2a. A notable feature is that the SPE at the positions of the probes THA and THE in the simulation domain seems to progress in a two-step manner. The transition occurs around substorm onset (~51 min.). The second step undergoes a steeper slope value than that in the first step. The time scale of the change is different. In the simulation, the risetime of the plasma pressure is about a few minutes, whereas in the observation, the risetime is about half of a minute. We will later discuss the reason of the time scale difference between the observation and the MHD simulation.

Figure 3 demonstrates plasma pressure as a function of X_{GSM} and time in equatorial plane ($Z_{GSM} = 0$ and $Y_{GSM} = -1$ *Re*) and at off equator ($Z_{GSM} = -1.5$ and $Y_{GSM} = -1$ *Re*). In the equatorial plane (Figure 3a), the plasma pressure starts to increase from tail region first, and high-pressure region (HPR) propagates earthward, at least, to X_{GSM}~−6 *Re*. After substorm onset, the HPR bifurcates. A major part continues to move earthward between 52 and 53 min and then after 53 min, it starts to expand both earthward and tailward. A subpart is separated on the outer side of the main one between $X_{GSM} = -8$ and −9 *Re* and is shown to retreat tailward. At $X_{GSM} = -7$ *Re*, the pressure will further increase after the onset, and then it starts to decrease after 53 min. At $X_{GSM} = -8$ *Re*, the first pressure peak corresponds to the peak of the main HPR then encounters the expanding of the main HPR. At $X_{GSM} = -9$ *Re*, the pressure variation undergoes a more complex way. The major part of the HPR results from the convergence of the thermal energy, and the sub part of it is associated with flow braking [*Shiokawa et al*., 1997; *Baumjohann*, 2002]. All these features are already described by *Tanaka et al*. [2010] in detail, so that we skip mentioning the detailed

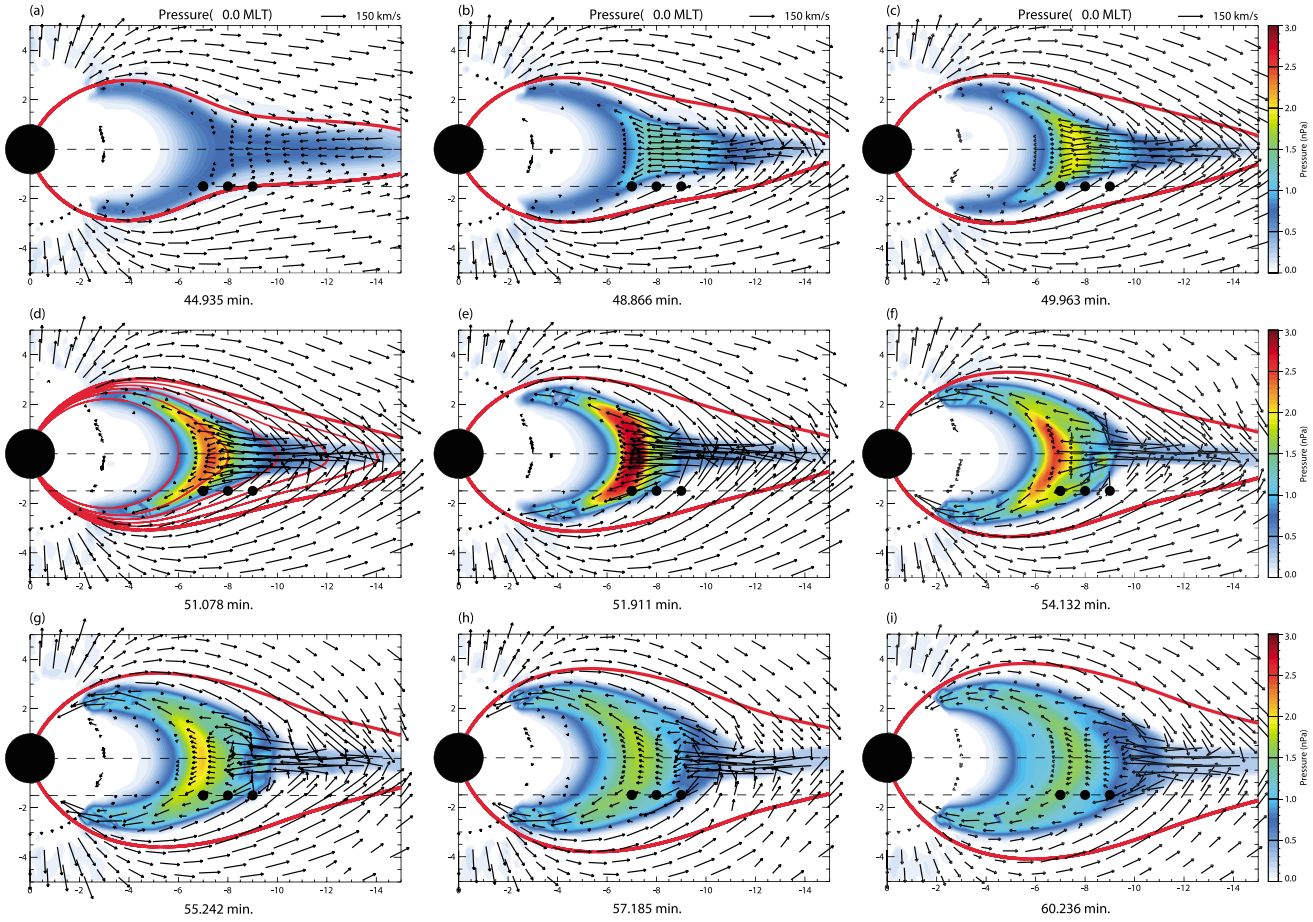

Figure 4. Development of simulated plasma pressure in the noon-midnight ($Y_{GSM} = 0$ *Re*) meridional plane around substorm onset (~51 min). The time sequence is from left to right and top to bottom. Pressure value is shown by color level. Velocity vector is shown by arrow. The three black solid circles indicate the coincident positions at four THEMIS probes in simulation domain (details are shown in Figure 1). The circles of probes THA and THE are overlaped, since the THA and THE have the same Z_{GSM} position in the simulation domain. The two horizontal dashed lines indicate the planes at $Z_{GSM} = 0$ and $Z_{GSM} = -1.5$ *Re*. The red solid line in each panel corresponds to the last closed magnetic field line (open-closed boundary), out of which the field lines are open. In Figure 4d, the red thin lines within the open-closed boundary are magnetic field lines that are traced from the equatorial plane at $X_{GSM} = -6$ to -14 *Re* with 2 *Re* interval.

feature of the HPR in the equatorial plane. At off equator (Figure 3b), the evolution of the pressure is different from that in the equatorial plane. It is shown that the pressure starts to increase around $X_{GSM} = -6.5$ *Re* just before the onset. The HPR expands both earthward and tailward after the onset. At $X_{GSM} < -6.5$ *Re*, the pressure increases first in the inner region, followed by the outer region.

Figure 4 demonstrates the evolution of plasma pressure in the noon-midnight ($Y_{GSM} = 0$ *Re*) meridional plane around substorm onset. Filled circles in each panel indicate the coincident locations of four THEMIS probes projected into the meridional-midnight plane. Since the projected positions of probes THA and THE are the same, they are overlapped. An arrow indicates the direction of plasma flow, and the length of the arrow indicates the flow speed projected into the noon-midnight plane. The two horizontal dashed lines refer to the planes at equator ($Z_{GSM} = 0$) and at off equator ($Z_{GSM} = -1.5$ *Re*). The red thick line corresponds to the last closed magnetic field line (open-closed boundary). During the substorm growth phase (Figures 4a–4c), the high-pressure region (HPR) is confined to around the equatorial plane and is broadly distributed around $X_{GSM} = -10$ *Re*. The plasma flow in the HPR is essentially earthward. The HPR is regarded as in the plasma sheet since it is located inside the open-closed boundary. Near the substorm onset (t~51 min), the plasma pressure in the HPR shows a further sudden increase. After reaching its peak at ~52 min, the HPR retreats tailward and extends along $+Z_{GSM}$ and $-Z_{GSM}$ directions. As a result, the HPR engulfs coincident positions at probes THC and THB. The interesting feature to be noted here is the reversion of flow direction from tailward to earthward before and after being engulfed by the HPR. Before the tailward retreat of the HPR,

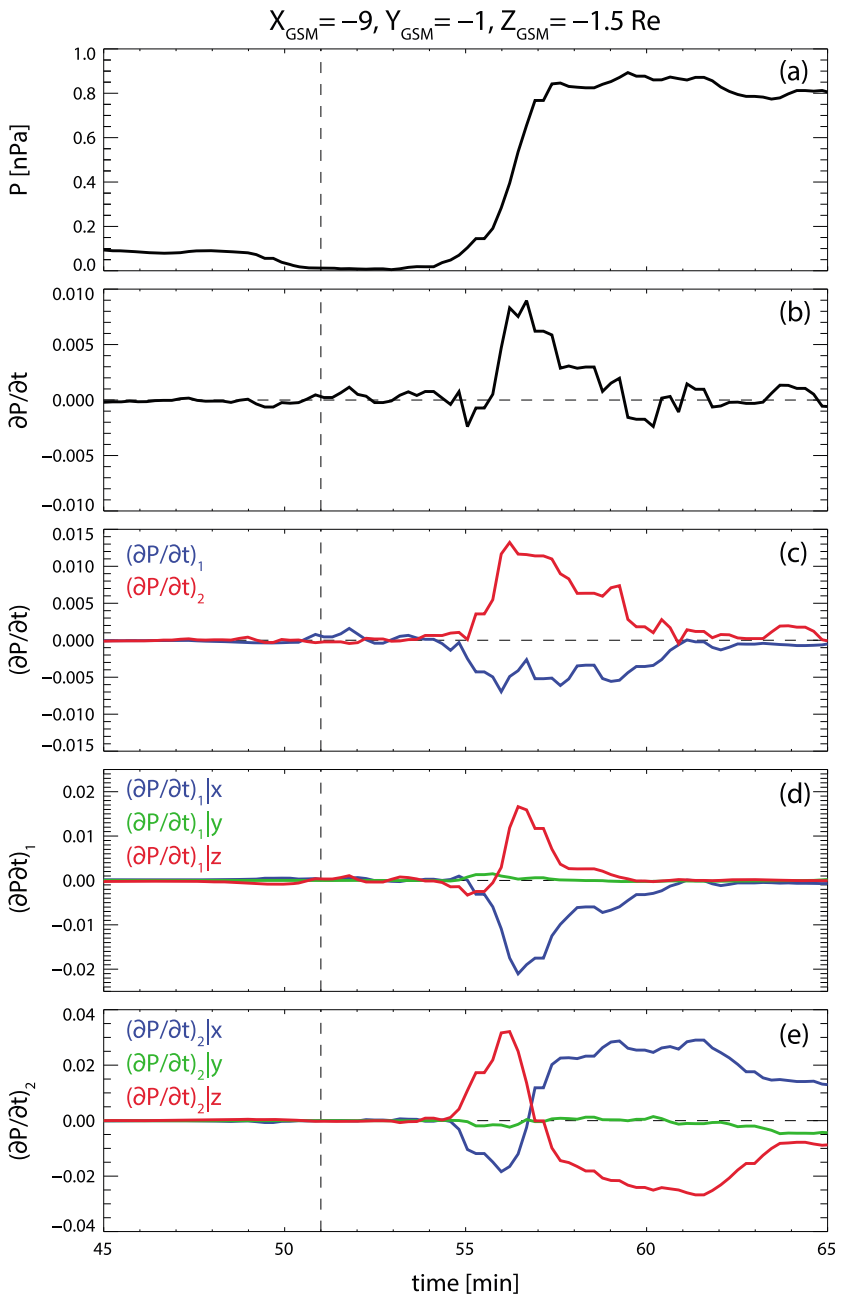

Figure 5. Temporal variation of (a) plasma pressure, (b) $\partial P/\partial t$ as defined by equation (1), (c) term 1 ($-\mathbf{V}\cdot\nabla P$) and term 2 ($-\gamma P\nabla\cdot\mathbf{V}$) on the right-hand side of the equation (1), three subterms of (d) the term 1, and of (e) the term 2. The vertical dashed line indicates the substorm onset defined by *AL* index [*Ebihara and Tanaka*, 2013].

the plasma at off equator outside of the HPR are moving tailward [*Tanaka et al.*, 2010] and toward the equatorial plane. The transition of the plasma flow direction occurs in the vicinity of the outer boundary of the HPR, which is not coincident with the open-closed boundary of magnetic field lines. The region of the closed magnetic field lines is extended outside of the outer boundary of the HPR. Hereinafter, we call the low-pressure and tailward plasma flow region a low-pressure region (LPR). Outside of the LPR, the magnetic field lines are open, that is, the lobe region. From Figure 4, it is found that the plasma flow is earthward in the HPR (near the equatorial plane), whereas the plasma flow is tailward in both LPR and lobe regions. In the HPR, the tension force ($(\mathbf{B}\cdot\nabla)\mathbf{B}/\mu_0$) resulting from the near-Earth neutral line accelerates the plasma earthward. In the LPR, the pressure gradient force ($-\nabla P$) along a field line provides a dominant

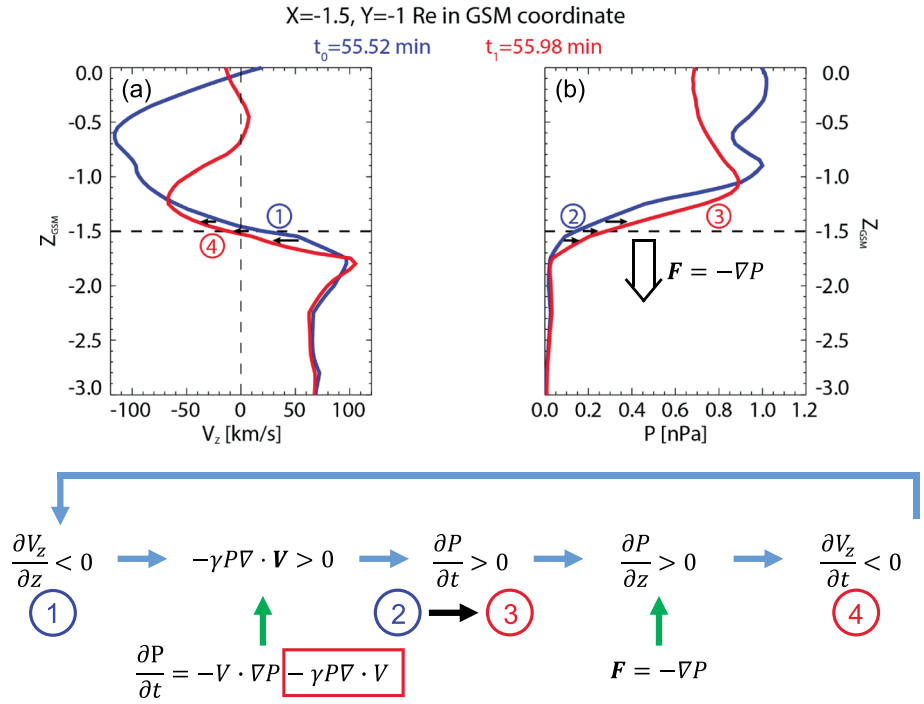

Figure 6. Schematic diagram showing the process leading to the pressure enhancement at off equator ($Z_{GSM} = -1.5\ Re$), the coincident position at probe B. (a) The simulated V_Z as a function of Z_{GSM} at $t_0 = 55.52$ min and $t_1 = 55.98$ min. (b) The simulated plasma pressure as a function of Z_{GSM} at t_0 and t_1.

tailward acceleration. Under the action of both forces in the X_{GSM}-Z_{GSM} plane, the reversion of the flow direction occurs.

To understand the evolution of plasma pressure, we evaluated the following adiabatic equation [*Tanaka et al.*, 2010]

$$\frac{\partial P}{\partial t} = -\mathbf{V}\cdot\nabla P - \gamma P\nabla\cdot\mathbf{V} \tag{1}$$

where γ is the specific heat ratio equal to 5/3. The first term on the right-hand side is regarded as advection of the plasma pressure, and the second one is regarded as compression or convergence of plasma flow. We refer them as $(\partial P/\partial t)_1$ and $(\partial P/\partial t)_2$, respectively. Figure 5 summarizes relevant quantities at off equator ($X_{GSM} = -9$, $Y_{GSM} = -1$, and $Z_{GSM} = -1.5\ Re$), corresponding to the coincident position of probe THB. Figure 5a shows the plasma pressure, indicating a large increase during the interval between ~55 and ~57 min. Figure 5b shows $\partial P/\partial t$ that is a sum of two terms on the right-hand side. Before 55 min, the $\partial P/\partial t$ is almost 0, which indicates that there is no significant pressure variation there. Because of unwanted numerical error in evaluating equation (1), the calculated $\partial P/\partial t$ is not exactly consistent with the pressure variation shown in Figure 5a. Figure 5c shows the $(\partial P/\partial t)_1$ term (blue) and the $(\partial P/\partial t)_2$ term (red), clearly indicating that the second term is responsible for the sudden enhancement of the pressure starting at ~55 min. The first term, however, results in a decrease in the pressure because of the earthward ($+X_{GSM}$ direction) advection of the pressure as shown in Figure 5d. The enhancement of the plasma pressure primarily comes from the Z component of the second term as shown in Figure 5e, that is, $-\gamma P(\partial V_Z/\partial z)$ at 55–57 min.

In Figure 6, we summarize velocity of Z component (V_Z) and plasma pressure (P) as a function of Z_{GSM} to illuminate this process near $Z_{GSM} = -1.5\ Re$. Note that the plasma pressure had been increased by the convergence of the thermal energy flux near the equatorial plane [*Tanaka et al.*, 2010]. As was demonstrated above, the term $-\gamma P(\partial V_Z/\partial z)$ is responsible to the sudden increase of the plasma pressure at off equator. Since the pressure value is positive, the negative value of $\partial V_Z/\partial z$ is responsible to the increase of the pressure. This means that the V_Z decreases with increasing Z_{GSM}. This condition is established by the existence of the

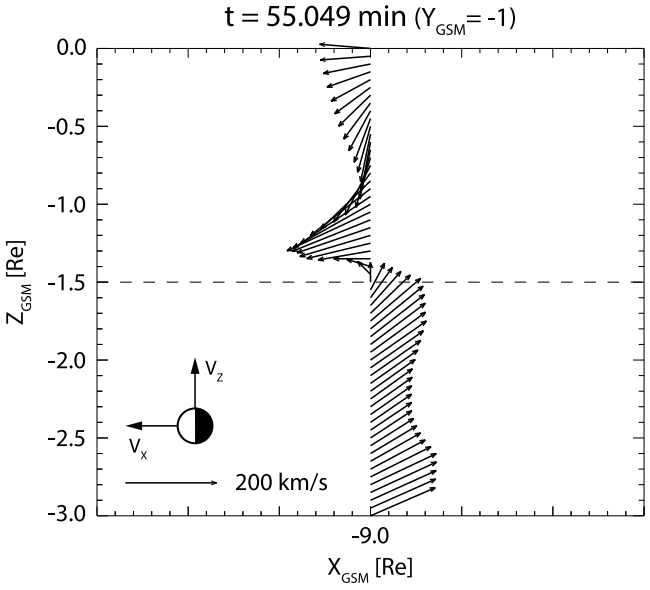

Figure 7. Plasma bulk velocity flow in the X_{GSM}-Z_{GSM} plane at 55.049 min. The flow velocities at $X_{GSM} = -9$ *Re*, $Y_{GSM} = -1$ *Re*, and $Z_{GSM} = -3$ to 0 *Re* are shown. The left-hand side refers to the earthward and the right-hand side refers to the tailward. Upward indicates the region close to the equator, and downward indicates that far from the equator.

shear of plasma flow. In a rough view from Figure 4, the plasma flow is earthward and away from the equatorial plane in high-pressure region (HPR), whereas the flow is tailward and toward the equatorial plane in low-pressure region (LPR). Figure 7 shows detailed velocity flow in X_{GSM}-Z_{GSM} plane at $Y_{GSM} = -1$ *Re*. It is obvious that there is a flow shear in the Z_{GSM} direction and that the flow in the X_{GSM} direction dominates that in the Z_{GSM} direction. The flow shear structure is moving downward away from the equator (in the southern hemisphere), which contributes to a negative $\partial V_Z/\partial z$. This configuration variation is also clearly seen in Figure 6a. Then, the pressure temporally increases according to equation (1), resulting in pressure gradient force acting on plasma downward ($-Z_{GSM}$ direction). This is indicated in Figure 6b. The dominance of the downward pressure gradient force (compared to upward $\mathbf{J}\times\mathbf{B}$ Lorentz force referring to equation (2)) causes acceleration of the plasma in the downward direction. This is shown in Figure 6a as a transition from a blue line to a red line. As a consequence of the iteration, the HPR expands downward as the flow shear moves downward, which is illustrated in Figure 8, and finally retreats tailward in a pattern like that in Figure 8b during later expansion phase and early recovery phase.

$$\rho\frac{d\mathbf{V}}{dt} = -\nabla P + \mathbf{J}\times\mathbf{B} \tag{2}$$

Figure 9a shows ion velocity of on board computed ESA moment data (in spin resolution) by probe THB (averaged over a 12 s window) with a comparison to that of MHD simulation (Figure 9b). Due to the contamination of background electrons, the ion velocity is uncertain after 15:41 UT, which is out of the period of interest (please refer to the supporting information for the details). In general, the simulation result shows a good agreement with the observational one in terms of the following. When probe THB encounters sudden pressure enhancement (SPE), V_Z (red line) undergoes a sharp decrease to a small positive value close to zero. Not like that shown in the simulation results, in which when the coincident position of the probe THB encounters the SPE, the V_Z does not only undergo a sharp decrease but also change the direction from equatorward (positive) to antiequatorward (negative). The difference between the simulation and the observation could be considered as a result of the smaller pressure gradient force obtained in the THEMIS observation, which could not provide enough deceleration on the V_Z to a negative value, compared to that of the simulation results. The velocity in the *X* component (blue line) is also shown as a sharp increase corresponding to the SPE. In both observation and simulation, the plasma flow changes its direction from tailward (negative) to earthward (positive). From the analysis on force balance along X_{GSM} axis, it is found that the V_X is negative referring to tailward flow before the SPE; however, it could be accelerated by the tension force $(\mathbf{B}\cdot\nabla)\mathbf{B}/\mu_0$. At ~55 min, the V_X was increased to positive value that indicates that a flow shear occurs from tailward to earthward, which corresponds to the start time of the SPE.

4. Discussion

By comparing Figures 2a and 2b, temporal variation of simulated plasma pressure by MHD simulation accords qualitatively with that observed by the THEMIS probes. The time scale of such variation in the simulation is

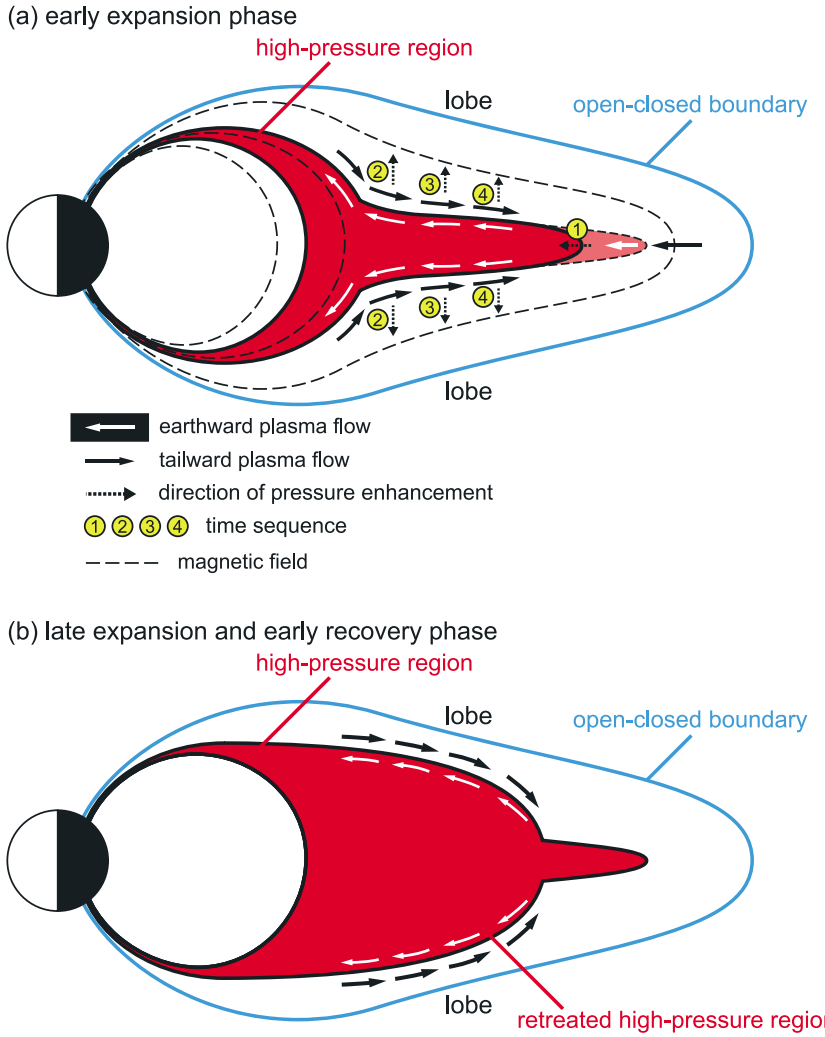

Figure 8. Schematic diagram illustrating the processes resulting in the pressure enhancement in the noon-midnight ($Y_{GSM} = 0\ Re$) meridinoal plane. The red region indicates the high-pressure region. The black dashed lines refer to magnetic field lines. The black and white solid arrow refers to the tailward and earthward plasma flows, respectively. The dashed arrow refers to the direction of the pressure enhancement. The number within the yellow circle indicates the time sequence of the high-pressure region (HPR) formation. (a) During the early expansion phase, numbers from 2 to 4 indicate the processes resulting in the tailward retreat of the HPR. However, number 1 in Figure 8a indicates the HPR formation before the onset. (b) Indicates the retreated HPR during the late expansion and early recovery phase.

longer than that seen in the observations by a factor of 2~3. A possible explanation could be considered as large mass density of plasma in the simulation. The large mass density may result in longer time scale than that observed by the THEMIS probes, because the large mass density causes a low acceleration rate that may require more running steps to get to convergence in the MHD simulation. However, we believe that the essentials may be hold regardless of the mass density. This issue will be resolved in the future.

Figure 4 shows that high-pressure region (HPR) tends to relax and retreat out tailward along the dipolar configuration after substorm onset. The HPR undergoing a tailward retreat will engulf the coincident position at probe THB in MHD simulation domain. As a glance, this process could be seen as an expansion. *Walker et al.* [1976, and references therein] reported increases and recoveries of the proton flux observed by the ATS 6 at synchronous orbit, which could be interpreted as substorm-associated boundary motion. The authors summarized three types of the boundary motion (Figure 12 of *Walker et al.* [1976]). The recovery of proton fluxes of 73 events in 75 observed by the ATS 6 could be associated with the boundary motion from north and tailward of the ATS 6 to equatorward and earthward (outside-in pattern). In this pattern, the fluxes of

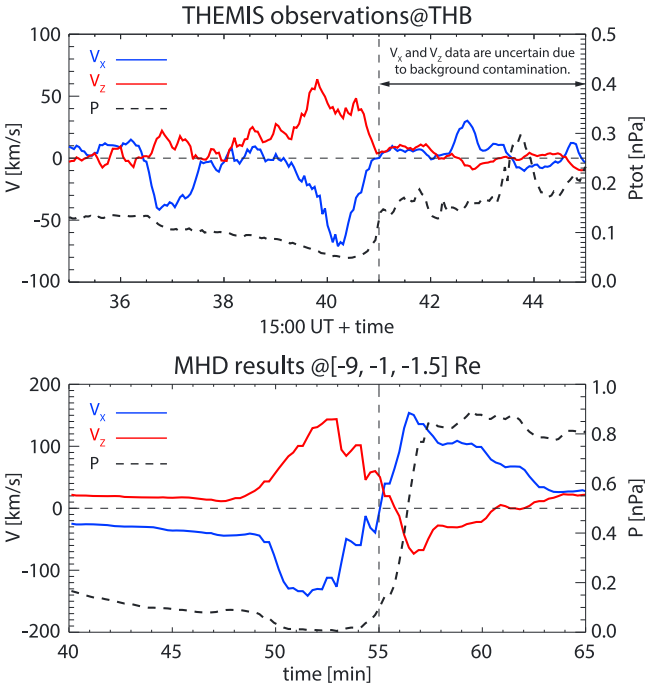

Figure 9. Time series of (a) ion velocity of on board computed ESA moment data in *X* (blue solid line) and *Z* (red solid line) components observed by probe B and (b) simulated velocity by global MHD simulation at coincident position at probe B. The thick dashed lines refer to (Figure 9a) observed total ion pressure and (Figure 9b) simulated plasma pressure. The dashed vertical lines indicate the time of sudden pressure enhancement. Due to the contamination of background electrons, the ion velocity is uncertain after 15:41 UT, which is out of the period of interest.

energetic particles enhance in the region tailward of the ATS 6 and then propagate earthward over the ATS 6. This pattern may not be the case that could be interpreted by our simulation results, since the reenhancement of the proton flux at the ATS 6 is not the consequence of the expansion of inner high flux region over the ATS 6. In another extreme pattern of the boundary motion, the ATS 6 may occasionally escape into the lobe region from the plasma sheet after the thinning motion of the boundary. Then, the spacecraft is engulfed from beneath by the expansion of the plasma sheet (inside-out pattern). This may be the same case as that shown in our simulation results.

Du et al. [2011] reported a substorm event on 9 March 2008, during which tailward flows in plasma sheet boundary layer (PSBL) were observed simultaneously by all THEMIS probes. The observations show that the occurrence of the tailward flows is dependent on the relative location close to the PSBL. Higher-speed tailward flows occur in the outer part of the PSBL, with movement into the PSBL, the flow speed seems to decrease, and in some cases, the tailward plasma flow could change to the earthward one. In the presented MHD simulation, the results show similar tendency. In the lobe region, plasma flows tailward. The flow speed decreases when it is approaching the inner part of the plasma sheet along $-X_{GSM}$ and $+Z_{GSM}$ at southern off equator. This could be interpreted as an acceleration by tension force along $+X_{GSM}$ and deceleration by pressure gradient force along $+Z_{GSM}$. When V_X is accelerated from negative to positive value, velocity shear occurs in the Z_{GSM} direction. Therefore, a boundary will be formed between tailward and earthward flows. This boundary could be seen as that which separates high-pressure region (HPR) and low-pressure region (LPR). The boundary is normally located in the plasma sheet (both in the substorm event on 1 March 2008 by THEMIS and the one by MHD simulation), in which case, the HPR and the LPR are both in the plasma sheet (closed field line). The development of the HPR in the case that the outer boundary of the HPR coincides with the open-closed boundary [*Du et al.*, 2011] will be investigated in the future.

5. Conclusions

1. We have found that the plasma pressure increased first in the inner region, followed by outer region, based on the THEMIS observations at off equator (Z_{GSM}~−1.5) in a substorm event that occurred on 1 March 2008.
2. The simulation results can reproduce the similar tailward retreat of the high-pressure region at approximate positions of the THEMIS probes in the simulation domain.
3. At off equator (Z_{GSM} = −1.5), only the tailward retreat of the SPE can be seen in the presented case. However, at the equator, there is an earthward propagation of the SPE first before the substorm onset.
4. From the viewpoint of force balance, the tailward retreat of the SPE could be explained by the propagation of high-pressure region in $-Z_{GSM}$ direction and from the inner to the outer along $-X_{GSM}$. The combination of the convergence of the plasma flow (velocity divergence along Z_{GSM} axis) and the pressure gradient force accounts for the propagation of the HPR along $-Z_{GSM}$.

Acknowledgments
This study was supported by KAKENHI, a grant-in-aid for Scientific Research (B) 24340119. We acknowledge NASA contract NAS5-02099 and V. Angelopoulos for the use of data from the THEMIS mission. Specifically, C.W. Carlson and J.P. McFadden for the use of ESA data; D. Larson and R.P. Lin for the use of SST data; and K.H. Glassmeier, U. Auster, and W. Baumjohann for the use of FGM data provided under the lead of the Technical University of Braunschweig and with financial support through the German Ministry for Economy and Technology and the German Center for Aviation and Space (DLR) under contract 50 OC 0302. Data from MHD simulation are available on request (Y. Ebihara: ebihara@rish.kyoto-u.ac.jp). The authors also would like to thank Yoshihara Omura and Shigeru Fujita for the fruitful discussions and Vassilis Angelopoulos for the support in reproducing the THEMIS data.

Michael Liemohn thanks the reviewers for their assistance in evaluating this paper.

References

Angelopoulos, V. (2008), The THEMIS mission, *Space Sci. Rev.*, *141*(1–4), 5–34.
Baker, D. N., T. I. Pulkkinen, V. Angelopoulos, W. Baumjohann, and R. L. McPherron (1996), Neutral line model of substorms: Past results and present view, *J. Geophys. Res.*, *101*, 12,975–13,010, doi:10.1029/95JA03753.
Baumjohann, W. (2002), Modes of convection in the magnetotail, *Phys. Plasma*, *9*(9), 3665–3667.
Baumjohann, W., G. Paschmann, and C. A. Cattell (1989), Average plasma properties in the central plasma sheet, *J. Geophys. Res.*, *94*, 6597–6606, doi:10.1029/JA094iA06p06597.
Baumjohann, W., G. Paschmann, T. Nagai, and H. Lühr (1991), Superposed epoch analysis of the substorm plasma sheet, *J. Geophys. Res.*, *96*, 11,605–11,608, doi:10.1029/91JA00775.
Du, A. M., et al. (2011), Fast tailward flows in the plasma sheet boundary layer during a substorm on 9 March 2008: THEMIS observations, *J. Geophys. Res.*, *116*, A03216, doi:10.1029/2010JA015969.
Ebihara, Y., and T. Tanaka (2013), Fundamental properties of substorm time energetic electrons in the inner magnetosphere, *J. Geophys. Res. Space Physics*, *118*, 1589–1603, doi:10.1002/jgra.50115.
Lui, A. T. Y., K. Liou, M. Nosé, S. Ohtani, D. J. Williams, T. Mukai, K. Tsuruda, and S. Kokubun (1999), Near-Earth dipolarization: Evidence for a non-MHD process, *Geophys. Res. Lett.*, *26*, 2905–2908, doi:10.1029/1999GL003620.
McFadden, J. P., C. W. Carlson, D. Larson, M. Ludlam, R. Abiad, B. Elliott, P. Turin, M. Marckwordt, and V. Angelopoulos (2008), The THEMIS ESA plasma instrument and in-flight calibration, *Space Sci. Rev.*, *141*(1–4), 277–302.
Nosé, M., T. Iyemori, M. Takeda, T. Kamei, D. K. Milling, D. Orr, H. J. Singer, E. W. Worthington, and N. Sumitomo (1998), Automated detection of Pi2 pulsations using wavelet analysis: 1. Method and an application for substorm monitoring, *Earth Planets Space*, *50*(9), 773–783.
Sergeev, V. A., M. A. Shukhtina, R. Rasinkangas, A. Korth, G. D. Reeves, H. J. Singer, M. F. Thomsen, and L. I. Vagina (1998), Event study of deep energetic particle injections during substorm, *J. Geophys. Res.*, *103*, 9217–9234, doi:10.1029/97JA03686.
Shiokawa, K., W. Baumjohann, and G. Haerendel (1997), Braking of high-speed flows in the near-Earth tail, *Geophys. Res. Lett.*, *24*, 1179–1182, doi:10.1029/97GL01062.
Tanaka, T., A. Nakamizo, A. Yoshikawa, S. Fujita, H. Shinagawa, H. Shimazu, T. Kikuchi, and K. K. Hashimoto (2010), Substorm convection and current system deduced from the global simulation, *J. Geophys. Res.*, *115*, A05220, doi:10.1029/2009JA014676.
Tsyganenko, N. A. (1989), A magnetospheric magnetic field model with a warped tail current sheet, *Planet. Space Sci.*, *37*(1), 5–20.
Walker, R. J., K. N. Erickson, R. L. Swanson, and J. R. Winckler (1976), Substorm-associated particle boundary motion at synchronous orbit, *J. Geophys. Res.*, *81*, 5541–5550, doi:10.1029/JA081i031p05541.
Wang, C.-P., L. R. Lyons, M. W. Chen, and R. A. Wolf (2001), Modeling the quiet time inner plasma sheet protons, *J. Geophys. Res.*, *106*, 6161–6178, doi:10.1029/2000JA000377.
Wing, S., Jesper W. Gjerloev, Jay R. Johnson, and R. A. Hoffman (2007), Substorm plasma sheet ion pressure profiles, *Geophys. Res. Lett.*, *34*, L16110, doi:10.1029/2007GL030453.
Xing, X., L. R. Lyons, Y. Nishimura, V. Angelopoulos, E. Donovan, E. Spanswick, J. Liang, D. Larson, C. Carlson, and U. Auster (2011), Near-Earth plasma sheet azimuthal pressure gradient and associated auroral development soon before substorm onset, *J. Geophys. Res.*, *116*, A07204, doi:10.1029/2011JA016539.
Xing, X., L. R. Lyons, X.-Z. Zhou, V. Angelopoulos, E. Donovan, D. Larson, C. Carlson, and U. Auster (2012), On the formation of pre-onset azimuthal pressure gradient in the near-Earth plasma sheet, *J. Geophys. Res.*, *117*, A08224, doi:10.1029/2012JA017840.
Yamaguchi, R., H. Kawano, S. Ohtani, S. Kokubun, and K. Yumoto (2004), Total pressure variations in the magnetotail as a function of the position and the substorm magnitude, *J. Geophys. Res.*, *109*, A03206, doi:10.1029/2003JA010196.